Upconversion phosphor thermometry for use in thermal barrier coatings

OPEN ACCESS
IOP Publishing
Measurement Science and Technology
Meas. Sci. Technol. **34** (2023) 064003 (14pp)
https://doi.org/10.1088/1361-6501/acc121

Upconversion phosphor thermometry for use in thermal barrier coatings

Henrik Feuk*, **Sebastian Nilsson and Mattias Richter**

Combustion Physics, Lund University, Lund, Sweden

E-mail: henrik.feuk@forbrf.lth.se

Received 5 January 2023, revised 28 February 2023
Accepted for publication 3 March 2023
Published 14 March 2023

Abstract

Measuring the temperature below the surface of a thermal barrier coating (TBC) using a thin phosphor layer is challenging primarily due to the absorption and scattering of laser excitation light and phosphor luminescence as they propagate through the coating. One way to increase phosphor luminescence could be to use upconversion phosphor thermometry, which is investigated in the current study. It is attractive because using longer excitation wavelengths reduces the absorption and scattering in TBCs as 8% wt. yttria-stabilize zirconia (8YSZ) generally has lower scattering and absorption coefficients around 1000 nm than at 532 and 355 nm. Therefore, the viability of upconversion to measure the temperature at the bottom of a TBC was evaluated for the first time and was compared with the more conventional downconversion phosphor thermometry. The current work involved an experimental study of several phosphors with lanthanides doped in the 8YSZ host, which were excited through downconversion by pulsed 355 nm and 532 nm laser light and through upconversion with 965 nm laser light. The YSZ:Er,Yb and YSZ:Ho,Yb phosphors show promise for upconversion phosphor thermometry. The experimentally acquired optical phosphor characteristics were used to simulate laser light and phosphor luminescence propagation in TBCs using Kubelka–Munk theory. This was to evaluate the signal strength with upconversion excitation compared to downconversion excitation. Upconversion excitation resulted greater signal strength from an embedded phosphor layer than 532 nm excitation and much higher than 355 nm excitation. Upconversion lifetime phosphor thermometry also resulted in improved phosphor lifetime temperature sensitivity. Coupled with reduced interference from background luminescence from impurities in TBCs with upconversion, it is a promising method for temperature measurements with the thermographic phosphor embedded in or underneath a TBC.

Keywords: thermal barrier coating, phosphor thermometry, upconversion, Kubelka–Munk

(Some figures may appear in colour only in the online journal)

1. Introduction

Thermal barrier coatings (TBCs) typically consist of a yttria stabilized zirconia (YSZ) topcoat secured to a metal substrate with a bond coat. The purpose of TBCs is to protect the metal substrate from high temperatures. With higher operating temperature, for example, in gas turbines, comes higher efficiency, but if the temperature of components becomes too high, the lifetime of TBC coated components can be significantly reduced [1]. Therefore, accurate temperature measurements in TBCs at the bond coat and the surface of the TBC can be used to balance the system's efficiency with the components' lifetime.

The phosphors in this study consist of 8YSZ as the host, which is widely used as the ceramic top coating of TBCs,

* Author to whom any correspondence should be addressed.

doped with trivalent lanthanides (Ln^{3+}), which replaces Y^{3+} content so that the 8.7% atomic percentage (8% weight) of rare earth elements remains constant in the TBC. With this method, the physical properties of the TBC material remain very similar while the optical properties of the lanthanide doped layer change.

Downconversion phosphor thermometry, i.e. excitation wavelength shorter than emission wavelength, with phosphor layers embedded on top of the bond coat layer and on the surface of TBCs, has been used [2–5]. In addition, downconversion measurements on uniformly lanthanide-doped TBC layers have also been performed [6, 7]. However, to the authors' knowledge, no study has been conducted to evaluate the use of upconversion phosphor thermometry, i.e. excitation wavelength longer than emission wavelength, for temperature measurements in a TBC.

Phosphor thermometry strategies using a uniformly doped TBC, in the hundreds of micrometres thick, results in issues with regards to the sensing depth not only in situations with temperature gradients in the TBC but also due to the temperature dependence of the absorption and scattering coefficients of the YSZ material [8, 9]. These temperature sensitivities do not influence the temperature measurements of a thin phosphor coating at the bottom of a TBC if one can assume uniform temperature in the phosphor layer and if the changes in absorption and scattering coefficients of the TBC with temperature do not drastically reduce the phosphor luminescence leaving the coating.

YSZ TBCs can contain impurities in the form of lanthanide ions, which make the TBC material optically active and can interfere with detecting the desirable phosphor luminescence signal [2]. This is particularly an issue when the phosphor layer is at the bottom of the TBC, as the excitation laser light is stronger at shallow depths into the TBC, and the path length of the stimulated luminescence is shorter if it is emitted at a shallow depth in the coating. Upconverting phosphor luminescence has previously been used to assess the delamination progression in TBCs [10]. Only a thin section on the bottom of a YSZ TBC was doped with Erbium and Ytterbium and excited using 980 nm laser light, and the 562 nm emission was used for delamination assessment. One benefit of upconversion luminescence in this application was the reduction in luminescence originating from rare earth impurities in the YSZ TBC. This is because most rare earth elements are not effectively excited by 980 nm without the Yb^{3+} sensitiser ion [10].

Kubelka–Munk simulations have been applied to describe laser light and downconversion phosphor luminescence propagation in TBCs [3, 11–13]. These models have been used to predict the temperature sensing depth in situations with uniformly lanthanide-doped TBC coatings and temperature gradients in the TBC [11]. This was performed using lifetime phosphor thermometry. These models also showed that an embedded phosphor layer underneath an undoped YSZ layer suffers from significant signal reduction. One potential benefit of using upconversion phosphor thermometry is the lower absorption and scattering of the excitation laser light in YSZ with laser light around 970 nm compared with 355 nm and 532 nm, which allows the laser light to penetrate deeper. Upconversion excitation at approximately 970 nm was therefore compared with 355 nm and 532 nm excitation using Kubelka–Munk modelling for three different 8YSZ TBC deposition processes, atmospheric plasma spray (APS), electron beam physical vapour deposition (EB-PVD), and suspension plasma spray (SPS) using literature values for the scattering and absorption coefficients of 8YSZ for the different deposition techniques. However, the quantum efficiency of phosphors with different excitation wavelengths must also be considered to evaluate the optimal excitation wavelength.

The purpose of this study is then to, for the first time, evaluate upconverting phosphor thermometry for use in TBCs by first characterising a range of phosphors and then simulating the situation where the phosphors YSZ:Er,Yb, YSZ:Er, and YSZ:Ho,Yb are applied in thin phosphor layers at the bottom of a TBC using Kubelka–Munk modelling.

2. Experimental setup

Only the 8YSZ $Zr_{0.913}Y_{0.087}O_{1.9565}$ host was used for the phosphors in the current study, where the Y^{3+} content was replaced by lanthanides to preserve the same physical properties as the common 8% weight Y^{3+} YSZ used in TBCs. For example, the composition of YSZ:Er,Yb with 1% Er^{3+}, and 3% Yb^{3+} is $Zr_{0.913}Y_{0.047}Er_{0.01}Yb_{0.03}O_{1.9565}$, the same as in [10]. YSZ:Er was selected because its luminescence has been shown to be insensitive to the gas oxygen environment [14] and because of its promise shown in previous work [15]. YSZ:Tm was selected due to the promise shown with Tm^{3+} doped in YAG [16]. YSZ:Er,Yb, YSZ:Ho,Yb, and YSZ:Tm,Yb were selected due to the efficient upconversion of Er,Yb, Ho,Yb, and Tm,Yb reported in literature [17–21]. The YSZ:Er,Yb phosphor has previously been used for upconversion lifetime phosphor thermometry using excitation at 1064 nm and was shown to have a temperature-sensitive decay time up until 1450 K, where the decay time was around 40 ns [22]. However, the most effective upconversion excitation wavelength is around 970 nm due to ytterbium's efficient energy transfer (ET) at that wavelength.

All the phosphors in this study were acquired from Phosphor Technology Ltd and are listed in table 1. The phosphors have a tetragonal crystalline phase (t-YSZ), which is not the tetragonal prime phase (t′-YSZ) that is typically used in TBCs as it resists transformation to other phases [23, 24]. However, the powders' tetragonal phase should not result in different optical phosphor characteristics compared to t′-YSZ phosphors in terms of emission spectra and phosphor luminescence lifetime in this study.

First, the phosphors were characterised with downconversion excitation. Then upconversion excitation and emission spectra for a selection of these phosphors was then also acquired. Finally, YSZ:Er,Yb and YSZ:Ho,Yb were calibrated for upconversion lifetime phosphor thermometry up to 1200 K.

The UV downconversion emission spectra were performed with the third harmonic (355 nm) from a 5 ns pulse duration

Table 1. Overview of phosphors studied and the way the phosphors were characterised. The excitation wavelengths are given in nm in the cells of the table. If it instead says N/A, the phosphor was not characterised with any wavelength.

Phosphor	Excitation wavelength for downconversion emission spectra (nm)	Excitation wavelength for downconversion lifetime calibration (nm)	Excitation wavelength for upconversion emission spectra (nm)	Excitation wavelength for upconversion lifetime calibration (nm)
YSZ:Er(1%),Yb(3%)	355, 532	355	965	965
YSZ:Ho(1%),Yb(3%)	355, 532	355	965	965
YSZ:Tm(1%),Yb(3%)	355	355	965	N/A
YSZ:Er(1%)	355, 532	355	N/A	N/A
YSZ:Tm(1%)	355	355	N/A	N/A

10 Hz Nd:YAG laser, and a RazorEdge (Semrock LP02-355RU-25) filter was used to remove laser light. In addition, downconversion emission spectra with the second harmonic output of the laser (532 nm) were also recorded with a notch filter (THORLABS NF5333-17) to remove elastically scattered 532 nm laser light. All emission spectra used the same laser pulse energy with a fluence of 16 mJ cm^{-2} for both 355 and 532 nm excitation and were recorded on an Avantes AvaSpec-ULS2048XL-EVO at room temperature. The presented emission spectra are averages of 100 single-shot emission spectra. The same 10 Hz laser system was used for downconversion lifetime calibrations with 355 nm excitation wavelength with the same calibration methodology developed in [25].

To obtain the upconversion excitation and emission spectra of the phosphors specified in table 1, a 90 ps pulse length optical parametric oscillator (OPO) output was scanned in the wavelength range between 890 and 1000 nm. The repetition rate of the laser system was 5 Hz, the mean laser pulse energy was 2 mJ, and the laser spot diameter was approximately 4 mm resulting in a laser pulse fluence of 16 mJ cm^{-2}. An 850 nm shortpass filter was used to remove the elastically scattered laser light from the emission spectra which were the average of 100 single-shot spectra.

After the optimal excitation wavelength for upconversion luminescence was determined, this wavelength was used to perform the upconversion lifetime calibration for the phosphors using the same laser system and the same laser energy and fluence settings as for the emission spectra recording. To investigate the general impact of using a 90 ps excitation source instead of a 5 ns pulse duration excitation laser source, the downconversion lifetime calibrations were performed once again for YSZ:Er,Yb, YSZ:Ho,Yb, and YSZ:Er with the same laser pulse energy, fluence, pulse duration, and phosphor luminescence collection system as for the upconversion calibration, but with a 355 nm excitation wavelength. This was performed to allow a comparison of the phosphor luminescence intensity difference with the two excitation wavelengths. However, it is important to note that the phosphor luminescence signal will scale with the square of the pulse excitation irradiance (W m^{-2}) with upconversion excitation as it is a two-photon process. On the other hand, downconversion excitation will scale linearly with pulse excitation irradiance.

All lifetime calibrations of the YSZ:Er,Yb, YSZ:Ho,Yb, and YSZ:Er phosphors used a 550 nm bandpass filter with full width at half maximum (FWHM) of 50 nm. For YSZ:Tm and YSZ:Tm,Yb a 458 nm bandpass with FWHM of 10 nm was used. All phosphors were coated on a Hastelloy C substrate, and the phosphor coating consisted of a mixture of HPC binder (ZYP coatings), ethanol, and phosphor powders for all the investigations in this study. The mean thickness of the coatings was 20 μm, which was measured with a thickness gauge (Elcometer 456) to ensure the expected coating thickness. When applying an embedded phosphor layer within a TBC it would ideally not be applied with a binder like HPC but instead with the same technique as the whole TBC is manufactured. This is to ensure minimal changes in the thermal properties of the TBC. However, it has been found that using an HPC binder does not change phosphor luminescence characteristics noticeably when compared with pure phosphor forms [26, 27]. Therefore, the gathered phosphor luminescence characteristics with HPC binder are representative of the behaviour of pure phosphors as well. However, the scattering coefficients of the 8YSZ powders mixed with the binder will not be representative of a pure 8YSZ coating.

3. Phosphor result and discussion

The emission spectra of all phosphors in figure 1 have emissions which were expected based on the lanthanides doped in 8YSZ. Note the strong emission around 965 nm for the phosphors with Yb^{3+}. The stronger infrared (IR) emission from Er,Yb than Ho,Yb is probably due to the better match of the energy levels between Yb^{3+} and Er^{3+} than Yb^{3+} and Ho^{3+} seen in figure 4.

YSZ:Er can be excited through downconversion with 355 nm, and 532 nm laser light and the phosphor's emission intensity has been found to be stronger with 532 nm excitation [15]. The decay time trend, however, was similar for YSZ:Er for both 355 nm and 532 nm excitation [15]. The good excitation efficiency with 532 nm is due to the proximity of Er^{3+} energy levels to 532 nm light, as demonstrated in figure 5. The room temperature emission spectrum with 532 nm excitation is plotted for YSZ:Er, YSZ:Er,Yb, and YSZ:Ho,Yb in the zoomed view in figure 1. The integrated emission intensity in the spectral range from 525 nm to 575 nm (the same range as the FWHM of the bandpass filter used for lifetime calibration) was 2.6, 2.2, and 1.8 times stronger for 532 nm than 355 nm excitation for YSZ:Er, YSZ:Er,Yb, and YSZ:Ho,Yb,

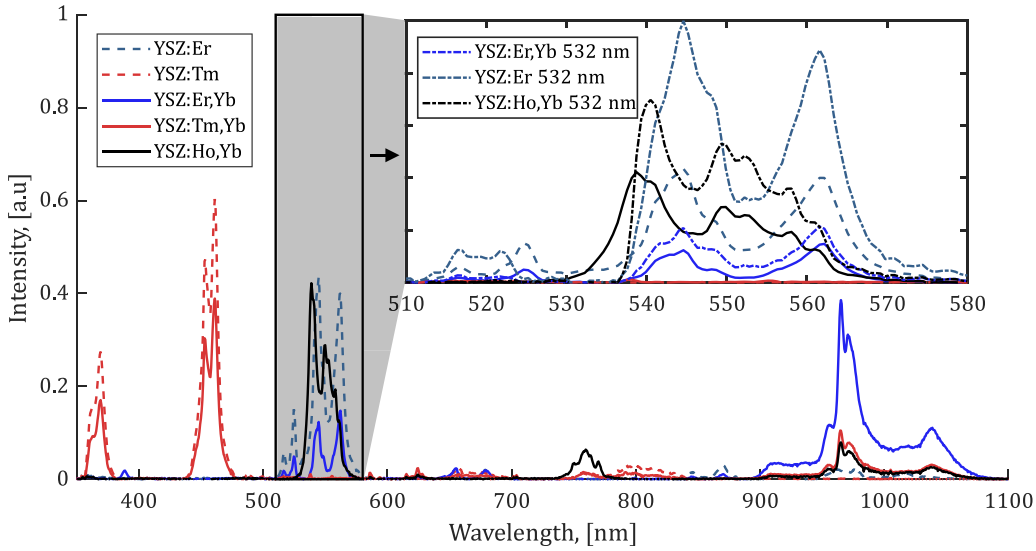

Figure 1. Downconversion phosphor emission spectrum with 355 nm excitation. The zoomed view between 510 and 580 nm includes the emission spectra with 532 nm laser excitation.

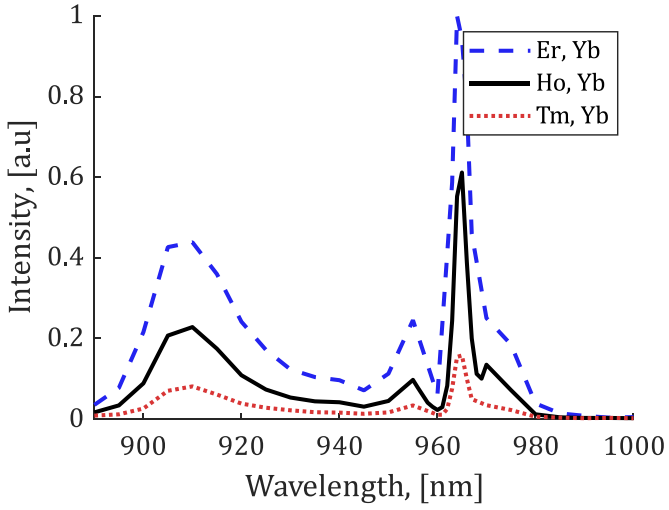

Figure 2. Upconversion excitation spectra of Yb^{3+} doped in 8YSZ phosphors.

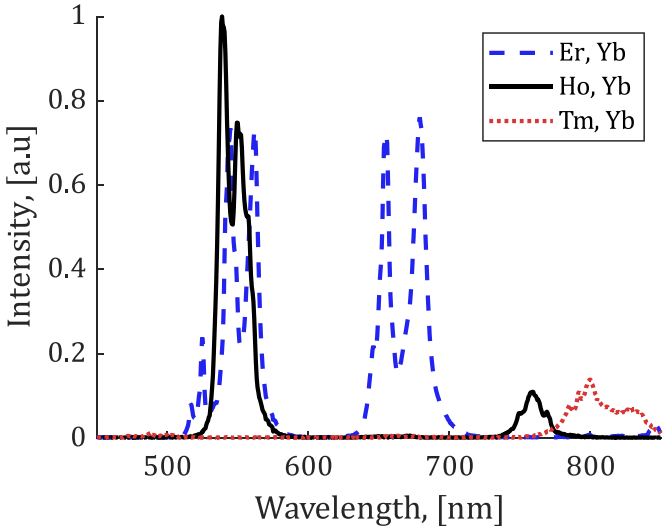

Figure 3. Upconversion emission spectrum of Yb^{3+} doped 8YSZ phosphors excited at 965 nm.

respectively. However, the IR emissions between 950 nm and 1100 nm for YSZ:Er,Yb with 532 nm excitation was 40% of the luminosity with 355 nm excitation and YSZ:Ho,Yb's emissions in the same spectral range could not be detected with 532 nm excitation. In a previous study YSZ:Er was found to be approximately 25 times more luminous for emissions around 550 nm with 532 nm excitation than 355 nm excitation, but the difference compared to the result shown in the present study is unclear beyond that 7YSZ was used in that study, and in the current study, 8YSZ is used [15].

The upconversion excitation spectra are shown in figure 2 for the three tested phosphors. The peak excitation wavelength was found to be 965 nm which is quite far from the often-used 980 nm excitation wavelength for phosphors with Yb^{3+}. However, this is the expected excitation peak for YSZ doped with Yb^{3+} [28, 29].

The emission spectra obtained using an excitation wavelength of 965 nm are shown in figure 3. The upconversion emission spectra of YSZ:Er,Yb shows a much stronger emission around 660 and 680 nm due to the $^4F_{9/2}$ to $^4I_{15/2}$ transition (figure 4) than with downconversion excitation in figure 1. YSZ:Ho,Yb's upconversion emission spectra is very similar to its downconversion emission spectrum. YSZ:Tm,Yb had very weak luminescence in the visible spectrum with upconversion; therefore, no upconversion lifetime calibration was performed with the phosphor.

The upconversion process of YSZ:Ho,Yb illustrated in figure 4 is enabled through ground state absorption (GSA) of the Yb^{3+} ion from ground state $^2F_{7/2}$ to excited state $^2F_{5/2}$ with the 965 nm excitation laser light. This energy is then transferred to the Ho^{3+} ion through energy transfer upconversion

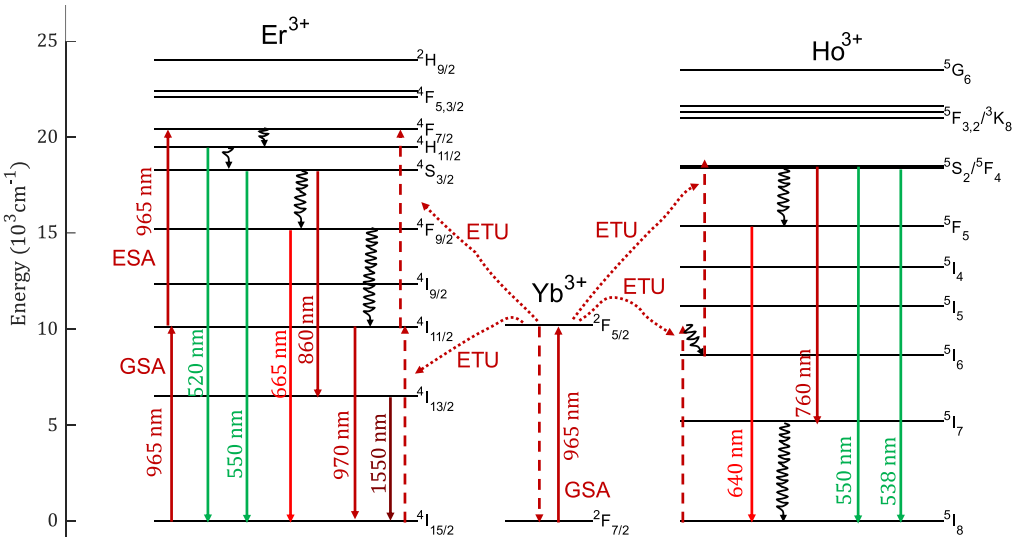

Figure 4. Energy level diagram with simplified energy transfer dynamics for upconversion luminescence. The transitions are based on [17–19, 30]. The wavy lines represent non-radiative transitions.

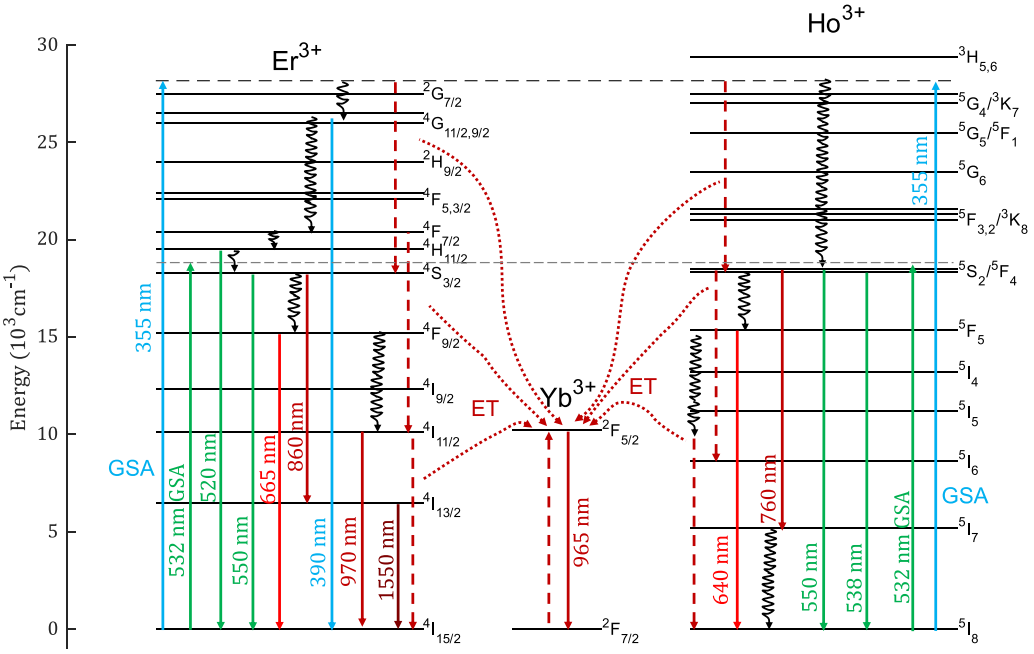

Figure 5. Energy level diagram with simplified energy transfer dynamics for downconversion luminescence with both 532 nm and 355 nm excitation. The transitions are based on [17–19, 30–32]. The wavy lines represent non-radiative transitions.

(ETU) to Ho^{3+} energy levels. The phosphor then decays with wavelengths shorter than the excitation wavelength. For YSZ:Er,Yb in figure 4, the same process occurs, but direct excitation of the Er^{3+} ion with 965 nm excitation is also possible through GSA and excited state absorption (ESA) processes.

When performing downconversion calibrations, the Yb^{3+} ETs are a loss in relation to the efficiency of visible phosphor luminescence emission, as illustrated in figure 5. This results in YSZ:Er,Yb being less luminous than YSZ:Er around 550 nm, as seen in figure 1. Therefore Yb^{3+} co-doping should only be performed if upconversion excitation will be used.

The results of the 90 ps laser pulse lifetime calibrations using upconversion and downconversion are shown in figure 6(a). No significant difference in the lifetime behaviour was observed between the nanosecond or picosecond excitation pulse lifetime calibrations. Therefore, the lifetime calibrations performed with the 5 ns laser are not shown in figure 6(a) except for YSZ:Tm, and YSZ:Tm,Yb because calibrations with the 90 ps laser were not conducted. A 550 nm bandpass filter with an FWHM of 50 nm was used for all calibrations with Ho^{3+} and Er^{3+}. This results in the $^5S_2/^5F_4$ to $^5I_8$ transition being characterised for Ho^{3+} and the $^3S_{3/2}$ to $^4I_{15/2}$ transition for Er^{3+}.

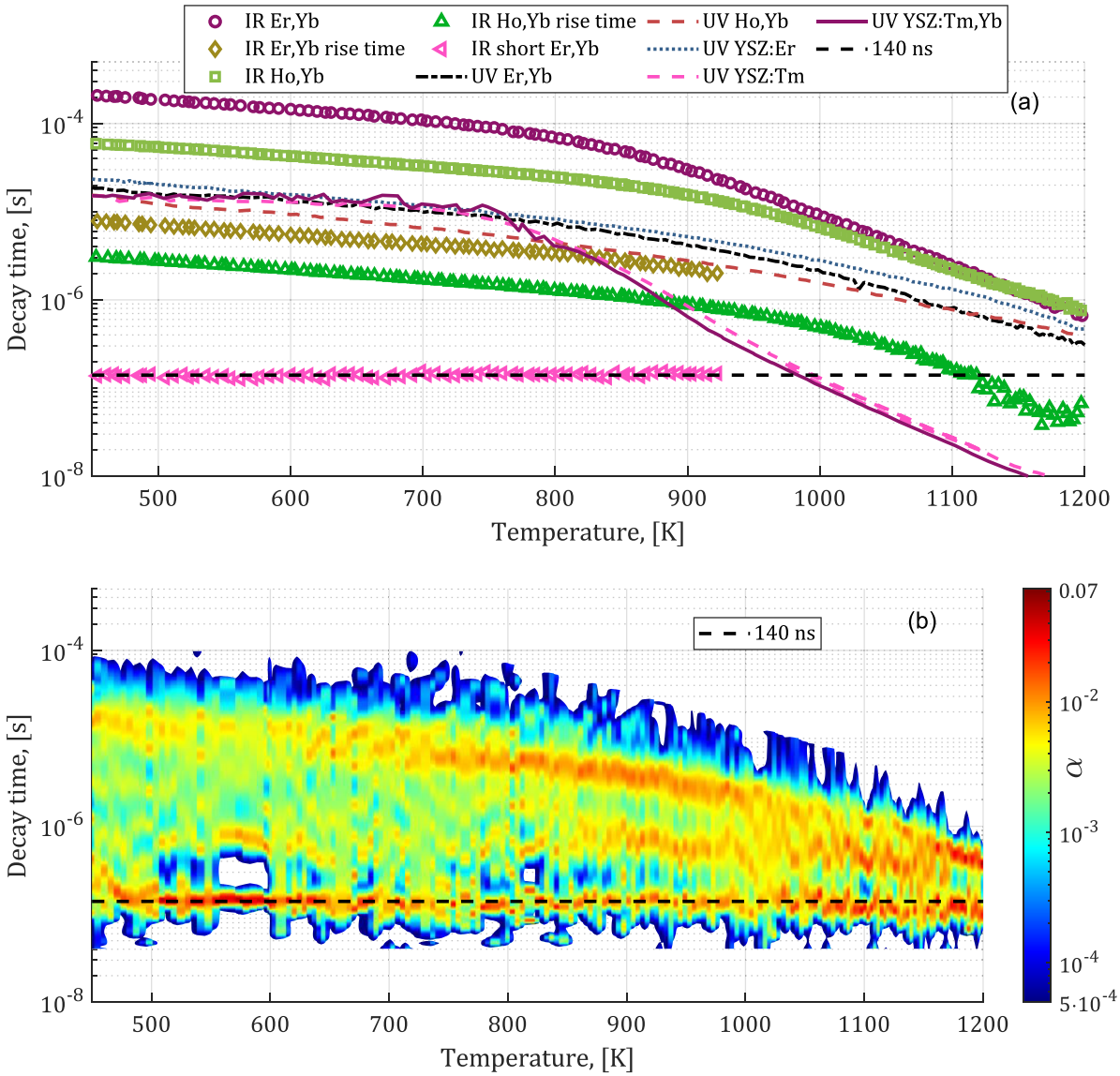

Figure 6. Temperature calibration in (a) of YSZ:Er,Yb and YSZ:Ho,Yb with both IR and UV excitation and only UV calibration for YSZ:Er, YSZ:Tm, and YSZ:Tm,Yb. For IR excitation, the 965 nm wavelength was used; for UV, the 355 nm excitation wavelength was used. The colour map in (b) results from decay time distribution analysis using the maximum entropy method [34, 35] on the YSZ:Er,Yb phosphor with 355 nm excitation. It shows that the same 140 ns lifetime component appears with 355 nm excitation of YSZ:Er,Yb as the short decay component of YSZ:Er,Yb with IR excitation.

The same laser excitation energy, excitation pulse duration, and signal collection system were used for YSZ:Er, YSZ:Er,Yb, and YSZ:Ho,Yb for both upconversion (IR data in figure 6(a)) and downconversion (UV data in figure 6(a)) to allow signal strength comparison. However, no excitation scan was performed around 355 nm excitation, so the downconversion phosphor luminescence intensity with UV light could most likely be improved with an OPO or dye laser system. The upconversion decay times are consistently longer than the downconversion decay times in figure 6(a). This is consistent with the typical behaviour that upconversion through ETU results in longer decay times than downconversion or direct excitation through GSA/ESA [32]. The longer decay time is caused by the emission energy level being populated through ET from a longer-lived state, in this case, the $^2F_{5/2}$ energy level of the Yb^{3+} ion [32].

The temperature sensitivity is improved with upconversion as the decay time becomes 320 times shorter for YSZ:Er,Yb from 450 K to 1200 K with upconversion, as shown in figure 6(a), but with downconversion, the decay time only becomes 60 times shorter. For YSZ:Ho,Yb, the decay time becomes 80 times shorter with upconversion and 40 times with downconversion in the same temperature range. For YSZ:Er with 355 nm excitation, the decay time became 50 times shorter in the same temperature range. Mono-exponential decay curve fitting was performed with an adaptable fitting window algorithm as described in [33], with $c_1 = 1$ and $c_2 = 6$. Rise times were measured with $c_1 = 0.5$ and $c_2 = 3.5$.

Table 2. Relative peak phosphor luminescence intensity for phosphor luminescence from 550 nm FWHM 50 nm. Data is based on emission spectra and lifetime calibrations. The values, in general, change with temperature, and the data extracted from the lifetime calibration data are averages in the temperature range from 500 to 1200 K. The emission spectra data is based on characteristics at room temperature in figures 1 and 3. Data is not presented with decimal places because the numbers vary with temperature, and such precision is not representative of the mean differences.

	Relative integrated phosphor luminescence			Relative peak phosphor luminescence intensity		
Excitation wavelength (nm)	YSZ:Er,Yb	YSZ:Ho,Yb	YSZ:Er	YSZ:Er,Yb	YSZ:Ho,Yb	YSZ:Er
355	1	4	4	1	5	3
532	2	7	11	2	9	9
965	7	11	—	1	3	—

The integrated phosphor luminescence and peak phosphor luminescence are compared in table 2 with YSZ:Er,Yb as the baseline phosphor. The values are based on the collected emission spectra and the lifetime calibrations. For YSZ:Er,Yb and YSZ:Ho,Yb, the integrated luminescence is significantly improved with upconversion excitation, but as the lifetimes also become longer (figure 6(a)), the peak phosphor luminescence reduces with upconversion excitation. The relative phosphor luminosity in table 2 is true for the laser pulse irradiance used in the current study. However, the relative luminosity may change with other pulse irradiances, as downconversion and upconversion excitation scale differently with excitation irradiance due to the former being a one-photon process and the latter being a two-photon process. For lifetime phosphor thermometry, the peak luminescence is of most importance as it is the factor which is directly coupled to the signal-to-noise ratio (SNR) of the signal. For the intensity ratio, the integrated signal is often of greatest importance. However, a long decay time will lead to greater background accumulation and background contributions to the signal. With 355 nm and 532 nm excitation, YSZ:Er and YSZ:Ho,Yb have very similar integrated phosphor luminescence. Because YSZ:Ho,Yb's decay time is shorter than YSZ:Er's decay time (figure 6(a)), it leads to YSZ:Ho,Yb's improved peak phosphor luminescence for the 355 nm and 532 nm excitation wavelengths relative to the integrated phosphor luminescence.

Both YSZ:Er,Yb and YSZ:Ho,Yb have long rise times in their lifetime behaviour when excited through upconversion. For YSZ:Ho,Yb, this rise time is resolvable in the entire temperature range of figure 6(a) as 'Ho,Yb rise time', but for YSZ:Er,Yb, the rise lifetime component could not be measured for temperatures above 920 K. This is because YSZ:Er,Yb has a short lifetime component in its luminescence with nanosecond rise time which conceals the relatively slow increase in luminescence intensity at higher temperatures. This short lifetime component of YSZ:Er,Yb is apparent in the zoomed-in view of the phosphor luminescence in figures 7(a) and (c), in contrast to YSZ:Ho,Yb in figures 7(b) and (d). The decay time of this component of YSZ:Er,Yb is approximately constant at 140 ns for all investigated temperatures, as shown in figure 6(a) with 'IR short Er,Yb'. This decay time was found by doing lifetime fitting exclusively on the initial decay curve in the zoomed-in phosphor luminescence in figures 7(a) and (c). The source of this constant decay time in the investigated temperature range is not known and further investigations are required to understand the reason for the lack of temperature dependence. However, the photomultiplier tube (PMT) was operated in a regime in terms of gain and phosphor luminescence intensity where detector effects are not likely to produce these results [36].

The fast initial rise in luminescence in YSZ:Er,Yb followed by a short decay with a 140 ns decay time is caused by the quick population of the higher energy levels of Er^{3+} through GSA from ground state $^4I_{15/2}$ to $^4I_{11/2}$ and then an ESA from $^4I_{11/2}$ to $^4F_{7/2}$ as illustrated in figure 4. This is possible for the YSZ:Er,Yb phosphor because Er^{3+} can be used for upconversion luminescence through GSA and ESA with excitation at approximately 980 nm without co-doping with Yb^{3+} [30, 37–39]. Therefore, direct population of Er^{3+} can be performed without transitions from Yb^{3+} ions. This population is much faster than the slow rise time component of YSZ:Er,Yb due to ETU from the $^2F_{5/2}$ to $^2F_{7/2}$ transition of the Yb^{3+} ion [40]. The luminescence increase behaviour of YSZ:Ho,Yb does not have this quick initial luminescence peak and subsequent decay. It only has the relatively slow rise time component due to the ETU from the Yb^{3+} ion because Ho^{3+} cannot effectively be excited by the 965 nm laser light directly.

The origin of the initial decay of YSZ:Er,Yb with upconversion in figures 7(a) and (c) with a 140 ns decay time is the same as the short decay components of YSZ:Er,Yb with 355 nm excitation. The decay components of YSZ:Er,Yb's decay with 355 nm excitation was resolved using the maximum entropy method (MEM) [34, 35] on the lifetime calibration of the phosphor. The result of the MEM analysis is the colour map in figure 6(b), where the colour bar is in log scale to better resolve the weighting, α, of the different lifetime components. A high α value means that the lifetime is significant in the luminescence decay. The short 140 ns is consistently a part of the decay time distribution of YSZ:Er,Yb decay with 355 nm excitation, which supports the idea that the initial decay of YSZ:Er,Yb with upconversion is a short decay component which also appears with downconversion excitation. The longer lifetime components of YSZ:Er,Yb's initial decay in the upconversion phosphor luminescence cannot be resolved in the decay curve due to them being overlapped with the luminescence increase caused by the ETU process.

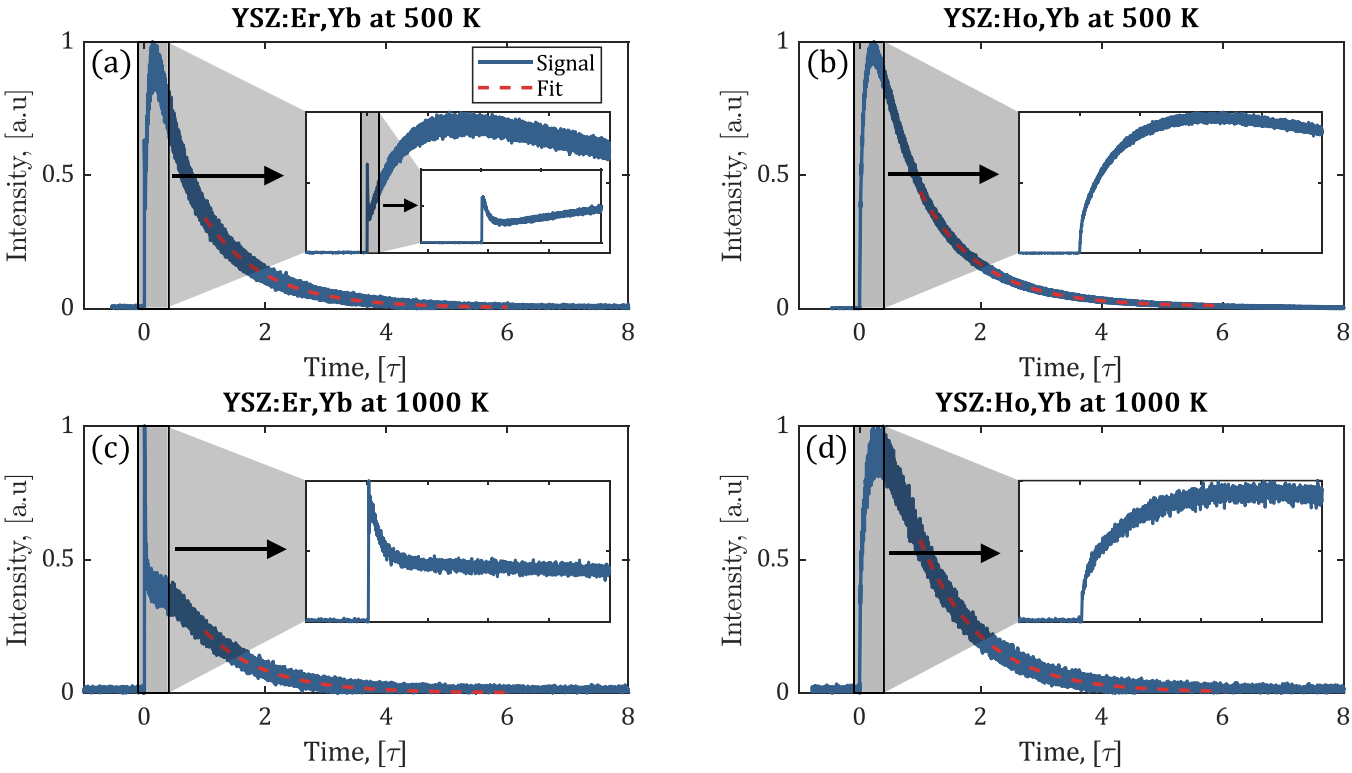

Figure 7. Appearance of upconversion decay curves. YSZ:Er,Yb at 500 K (a) and 1000 K (c). YSZ:Ho,Yb at 500 K (b) and 1000 K (d). The time scale on the x-axis was normalised based on the measured lifetime shown in figure 6(a). The short-lived luminescence around time 0 s was removed for improved clarity of the phosphor luminescence.

4. Kubelka–Munk model

Upconversion excitation of an embedded phosphor layer in a TBC with light at approximately 965 nm was compared with 355 nm and 532 nm excitation using Kubelka–Munk modelling for three different 8YSZ TBC deposition processes APS, EB-PVD, and SPS. The Kubelka–Munk model is a one-dimensional light-propagation model appropriate for highly scattering and weakly absorbing media [41] which is the case for 8YSZ TBCs. The governing equation for the propagation of the laser light in such media is:

$$\frac{\mathrm{d}}{\mathrm{d}x}\begin{Bmatrix} I_{\mathrm{laser}} \\ J_{\mathrm{laser}} \end{Bmatrix} = \begin{bmatrix} -(K_{\mathrm{laser}}+S_{\mathrm{laser}}) & S_{\mathrm{laser}} \\ -S_{\mathrm{laser}} & K_{\mathrm{laser}}+S_{\mathrm{laser}} \end{bmatrix} \times \begin{Bmatrix} I_{\mathrm{laser}} \\ J_{\mathrm{laser}} \end{Bmatrix} \quad (1)$$

where I_{laser} is the laser intensity propagating into the coating and J_{laser} is the laser intensity propagating out of the coating. S_{laser} is two times the scattering coefficient, s_{laser}, and K_{laser} is two times the absorption coefficient of the laser light, k_{laser}. S and K are used instead of s and k to account for the diffuse nature of the laser light propagating in the TBC. In situations with a phosphor in the TBC, some of the absorbed energy is converted to phosphor luminescence. The amount of luminescence is determined by the efficiency of laser intensity conversion to the phosphor emission wavelength region of interest.

The governing equation for phosphor luminescence is:

$$\frac{\mathrm{d}}{\mathrm{d}x}\begin{Bmatrix} I_{\mathrm{phos}} \\ J_{\mathrm{phos}} \end{Bmatrix} = \begin{bmatrix} -(K_{\mathrm{phos}}+S_{\mathrm{phos}}) & S_{\mathrm{phos}} \\ -S_{\mathrm{phos}} & K_{\mathrm{phos}}+S_{\mathrm{phos}} \end{bmatrix} \times \begin{Bmatrix} I_{\mathrm{phos}} \\ J_{\mathrm{phos}} \end{Bmatrix} + \begin{bmatrix} \frac{q\cdot K_{\mathrm{laser}}}{2} & \frac{q\cdot K_{\mathrm{laser}}}{2} \\ -\frac{q\cdot K_{\mathrm{laser}}}{2} & -\frac{q\cdot K_{\mathrm{laser}}}{2} \end{bmatrix} \times \begin{Bmatrix} I_{\mathrm{laser}} \\ J_{\mathrm{laser}} \end{Bmatrix} \quad (2)$$

where the second term is how luminescence is induced in the coating, where q is a term related to the quantum efficiency in the conversion of laser intensity to the phosphor luminescence intensity for the phosphor emission line of interest. This is often considered a constant for downconversion excitation. However, the excitation efficiency with upconversion will in general depend on the laser intensity due to it being a multi-photon process. The propagation of phosphor luminescence is described in the first term where I_{phos} is the phosphor luminescence intensity propagating into the coating and $J_{\mathrm{phos}}$is the luminescence intensity propagating out of the coating. S_{phos} is two times the scattering coefficient, s_{phos}, and K_{phos} is two times the absorption coefficient of the luminescence, k_{phos}. S and K are used instead of s and k to account for the diffuse phosphor luminescence propagation in the TBC. The differential equations in equation (2) were solved using appropriate boundary conditions discussed in [11, 12].

Table 3. Absorption and scattering values used in modelling. Data on 8YSZ APS and EB-PVD is primarily from [42] and supplemented with [8]. SPS data is from [43]. The absorption at 355 nm for the SPS coating is taken from the APS absorption data, as the absorption values of SPS at low values are not shown in the study [43].

		APS		EB-PVD		SPS	
Wavelength (nm)	Value range	Absorption (M^{-1})	Scattering (M^{-1})	Absorption (M−1)	Scattering (M^{-1})	Absorption (M^{-1})	Scattering (M^{-1})
355	High	$1.5{\cdot}10^3$	$1.45{\cdot}10^5$	$1.6{\cdot}10^3$	$12{\cdot}10^4$	$1.5{\cdot}10^3$	$11{\cdot}10^5$
	Low	$0.75{\cdot}10^3$	$1.05{\cdot}10^5$	$0.7{\cdot}10^3$	$7{\cdot}10^4$	$0.75{\cdot}10^3$	$10{\cdot}10^5$
525–575	High	270	$1.35{\cdot}10^5$	$1.2{\cdot}10^3$	$4{\cdot}10^4$	90	$8.5{\cdot}10^5$
	Low	90	$0.95{\cdot}10^5$	$0.3{\cdot}10^3$	$2{\cdot}10^4$	30	$8.0{\cdot}10^5$
965	High	100	$1.10{\cdot}10^5$	$1.2{\cdot}10^3$	$1{\cdot}10^4$	70	$5.0{\cdot}10^5$
	Low	10	$0.75{\cdot}10^5$	$0.2{\cdot}10^3$	$0.6{\cdot}10^4$	30	$4.5{\cdot}10^5$

5. Modelling

The values for the absorption and scattering coefficients for the APS, EB-PVD, and SPS deposition techniques were taken from the literature. For each TBC application process, three excitation wavelengths were simulated, 965 nm, 532 nm, and 355 nm. The scattering and absorption values for the different TBC application processes and wavelength ranges can be seen in table 3. The range 525–575 nm represents the range of scattering and absorption values for the phosphor luminescence and 532 nm laser excitation light. The upper and lower range of coefficients is partly based on variations due to different porosities in TBCs with the same coating application technique, but also differences in literature values in some instances. EB-PVD has the lowest scattering coefficient of the three coating techniques, and SPS has the highest. SPS generally has the lowest absorption coefficient, and EB-PVD has the highest. These differences result from how the TBC materials are structured with the coating techniques, where the columnar microstructure of EB-PVD results in a relatively low scattering coefficient and increases absorption coefficient relative to APS, which has a laminar microstructure [42]. The scattering and absorption coefficients in table 3 are valid for a perpendicular angle of incidence of the laser light to the TBC surface. Other angles of incidence could lead to different scattering and absorption coefficients, especially for EB-PVD, which is anisotropic. The pore size distribution with SPS results in a smaller mean diameter than APS, leading to more pores and pore interfaces acting as scattering sites [43] and resulting in SPS having higher scattering coefficients than APS.

Previous Kubelka–Munk simulations for YSZ TBCs in the context of lifetime phosphor thermometry have used reference data where the scattering coefficients of both APS and EB-PVD were lower towards the UV than the visible region, but these coefficients were from 7YSZ [11, 44, 45]. The scattering coefficients for 8YSZ are higher in the UV than for 7YSZ, leading to poor UV light penetration through 8YSZ coatings.

The Kubelka–Munk modelling assumes isotropic scattering, which is generally not true for EB-PVD due to its columnar microstructure, which also results in the scattering coefficient increasing deeper into the TBC [45]. Additionally, the averaged scattering coefficients in EB-PVD coatings increase with thickness of the coating as this affects the columnar grain diameter [42]. The anisotropic nature of EB-PVD coatings has previously been accounted for by increasing the scattering coefficient deeper into the TBC to improve Kubelka–Munk modelling accuracy [46]. However, this was not performed in the current study due to the difficulty in defining appropriate scattering coefficients at different depths. The scattering and absorption values in table 3 for EB-PVD have higher uncertainty than the other coating techniques due to the anisotropic nature of the coating and due to the difficulty of separating scattering and absorption effects in the UV to visible region.

In total, 1215 different scenarios were simulated as the lower and upper bound values in each cell of table 3 were used in addition to the average of the upper and lower bound values. By simulating all these different scenarios, one understands the range of results possible based on the variation in TBC scattering and absorption coefficients. The significant variations are mainly a result of different porosities of 8YSZ in the TBC. A low porosity leads to higher absorption, but lower scattering and high porosity lead to lower absorption and increased scattering [42]. In addition, the pore architecture, meaning size distributions and arrangement of grain boundaries, also affects the scattering and absorption coefficients. The scattering coefficients are consistently larger than the absorption coefficients which is needed for the Kubelka–Munk model to be accurate. Therefore, if absorption and scattering coefficients are similar, one should use the four-flux model instead for improved accuracy [41].

The 965 nm laser light consistently has the lowest absorption and scattering coefficients in table 3, which should allow the laser light to penetrate deeper into TBC coatings. Based on the absorption increase of 980 nm light due to Yb^{3+} doping in various hosts, an absorption coefficient increase of 400 m^{-1} for 3% Yb^{3+} doping in YSZ is reasonable [47–50]. Additionally, it was found that 0.5% and 6.5% of Yb^{3+} doped in YSZ resulted in absorption coefficients of 163 m^{-1} and 1844 m^{-1} with 966 nm excitation light, respectively [28]. Therefore, a lower estimate of 300 m^{-1} and a high estimate of 800 m^{-1} are reasonable estimates of the absorption coefficient increases caused by 3% Yb^{3+} doping for the 965 nm excitation wavelength. This value is added to the absorption coefficient in table 3 for the absorption of 965 nm light in a Yb^{3+} doped TBC layer. No increase in absorption coefficients was accounted for due to lanthanide doping for the 532

and 355 nm excitation wavelengths because the laser excitation wavelength was not tuned to perfectly overlap with a specific phosphor transition. The actual absorption coefficient for doped 8YSZ with 355 nm and 532 nm excitation may therefore be slightly different from the values reported in table 3. The quantum efficiency factor q in equation (2) was set to 0.5 for all three excitation wavelengths as in previous studies [11, 12], but it has no impact on the relative luminescence values in this study as it is just a multiplicative constant. Therefore, the quantum efficiency dependence on laser intensity with upconversion excitation is not captured in the Kubelka–Munk simulations. The reflectance at the thermally grown oxide layer interface is assumed to be 20% [10].

In uniformly phosphor-doped TBC and temperature gradients in the coating, the phosphor luminescence originates from a range of temperatures. Therefore, the resulting luminescence will contain components with varying decay times representing locally different temperatures [11, 12]. Due to the different absorption characteristics of the UV and IR excitation laser light, one could potentially use that to have different sensing depths with two excitation depths. If one knows the sensing depth of the two excitation wavelengths, one can then measure the temperature gradient in the TBC. However, this methodology requires careful calibration of the phosphor TBC or very accurate absorption and scattering parameters (including temperature dependence) to provide accurate temperature gradient measurements. This is because a TBC material's absorption and scattering parameters are not constant with temperature [8, 9]. The use of dual depth sensing to measure temperature may be feasible but exciting an embedded thin phosphor coating is a conceptually simpler technique which could be complimented with a thin phosphor layer or pyrometry measurement on the surface of the TBC to get the temperature gradient in a TBC. Therefore, the situation with a thin phosphor layer at the bottom of a TBC but on top of the metal oxide layer is simulated in the present study with a comparison between 355, 532, and 965 nm excitation wavelengths. The simulated TBC coating consists of an undoped 180 µm thick 8YSZ coating on top of a 20 µm 8YSZ coating doped with different combinations of Yb^{3+} and Er^{3+} or Ho^{3+}, which sits on the bond coat. This results in a total thickness of 200 µm of the simulated 8YSZ TBC coating.

6. Modelling results and discussion

The laser intensity into and out of an APS TBC is shown in figure 8(a), and the phosphor luminescence, assuming constant temperature in the phosphor layer underneath the TBC, in figure 8(b). Due to the relatively thin phosphor layer, a temperature gradient in the TBC will not alter the results fundamentally. Therefore, this simulation will also give a general indication of the absorption and scattering in that situation. The 355 nm laser wavelength is much more quickly absorbed in the TBC than the IR and 532 nm excitation light (figure 8(a)). This results in greater phosphor luminescence for the IR and 532 nm excitation than for 355 nm in figure 8(b). The error bars and the shaded regions show the standard deviation in the laser and phosphor luminesce at different parts of the coating based on the range of absorption and scattering coefficients simulated. The result of most interest in figure 8 is the intensity of the phosphor luminescence leaving the surface of the TBC shown in figure 8(c). This is the intensity of J_{lum} at the surface of the coating. Figure 8(c) shows that 965 nm excitation results in approximately seven times stronger mean phosphor luminescence than 532 nm. 355 nm excitation is three times weaker than 532 nm excitation due to the higher scattering and absorption for 355 nm excitation.

With the EB-PVD technique in figure 9, the lower scattering leads to higher laser intensities deeper in the coating and, in turn, greater conversion of laser pulse energy to phosphor luminescence. The mean phosphor luminescence leaving the TBC, as seen in figure 9(c), is six times stronger for 965 nm excitation than for 532 nm excitation, and the 355 nm excitation was much weaker than both.

With the SPS technique in figure 10, very high scattering values lead to very low laser intensities deeper in the coating, as most laser light is not absorbed in the TBC but scattered out of the surface of the TBC, as seen by the high values of the J_{laser} in figure 10(a) for all excitation wavelengths. The mean phosphor luminescence leaving the TBC was 20 times larger with upconversion excitation than 532 nm, as indicated in figure 10(c).

The 965 nm excitation is the brightest excitation wavelength assuming constant conversion efficiency from laser intensity to phosphor luminescence intensity, as seen in (c) for figures 8–10. The 532 nm excitation results in less bright phosphor luminescence, but the phosphor luminescence with 355 nm excitation is far lower than the 532 nm and 965 nm excitation sources. However, as seen by the error bars in (c) for figures 8–10, the range of simulated coefficients profoundly impacts the phosphor luminescence leaving the TBC. The phosphor luminescence intensity with 965 nm excitation leaving the TBC with the EB-PVD coatings is approximately 7 and 50 times stronger than the APS and SPS application techniques, respectively. This is due to the overall lower scattering coefficients for the EB-PVD coatings compared to the other coating application techniques.

To determine the optimal excitation wavelength for an embedded thin phosphor coating, be it 532 nm or 965 nm, one needs to account for the efficiency with which the phosphor is excited by the laser light. Therefore, the relative peak luminescence intensity results from table 2, which contains information about the relative conversion efficiency of laser light to phosphorescence, were multiplied by the luminescence leaving the TBC surface in (c) for figures 8–10, and the results are presented in figure 11 below. YSZ:Ho,Yb excited with 965 nm is the configuration in figure 11 that results in the strongest phosphor luminescence intensity for all TBC application techniques covered in this study owing to the better penetration of 965 nm excitation laser light and the relatively efficient emission from YSZ:Ho,Yb. Figure 11 highlights again that the EB-PVD TBC application method results in superior phosphorescence luminescence leaving the surface of the TBC.

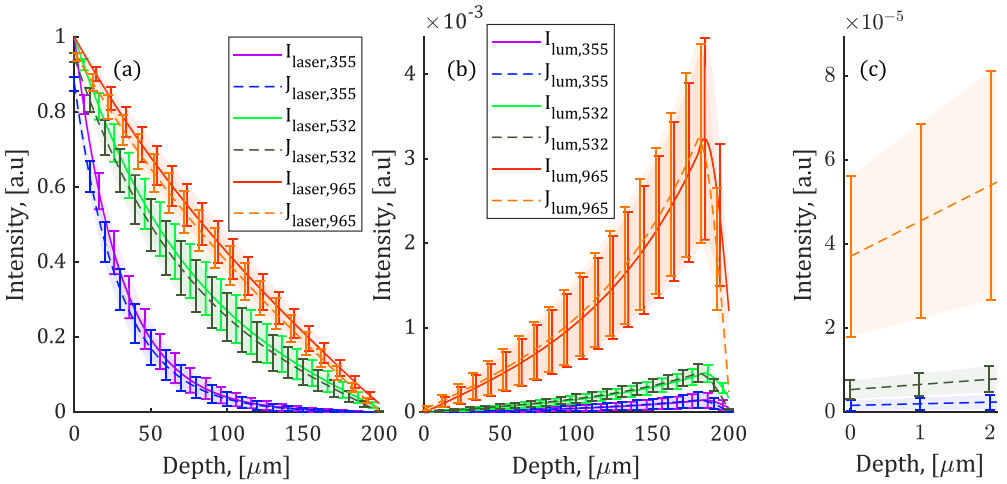

Figure 8. APS TBC application method. Laser intensity at different depths in the TBC (a) and phosphorescence intensity at different depths with phosphor-doping only in the bottom 20 µm of the 200 µm deep TBC (b). Excitation with UV (355 nm), visible (532 nm) and IR (965 nm) is shown for emission at 550 nm. (c) Shows the phosphor luminescence close to the TBC surface propagating out of the coating.

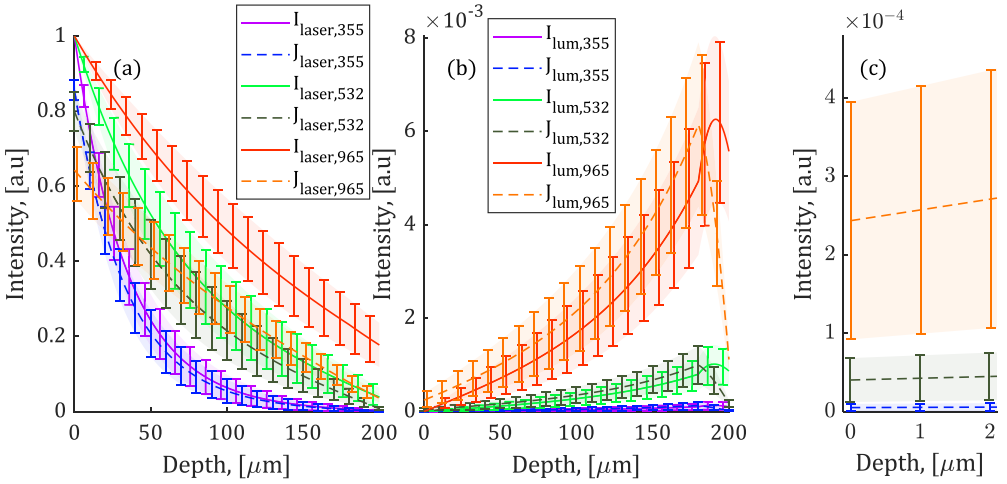

Figure 9. EB-PVD TBC application method. Laser intensity at different depths in the TBC (a) and phosphorescence intensity at different depths with phosphor-doping only in the bottom 20 µm of the 200 µm deep TBC (b). Excitation with UV (355 nm), visible (532 nm) and IR (965 nm) is shown for emission at 550 nm. (c) Shows the phosphor luminescence close to the TBC surface propagating out of the coating.

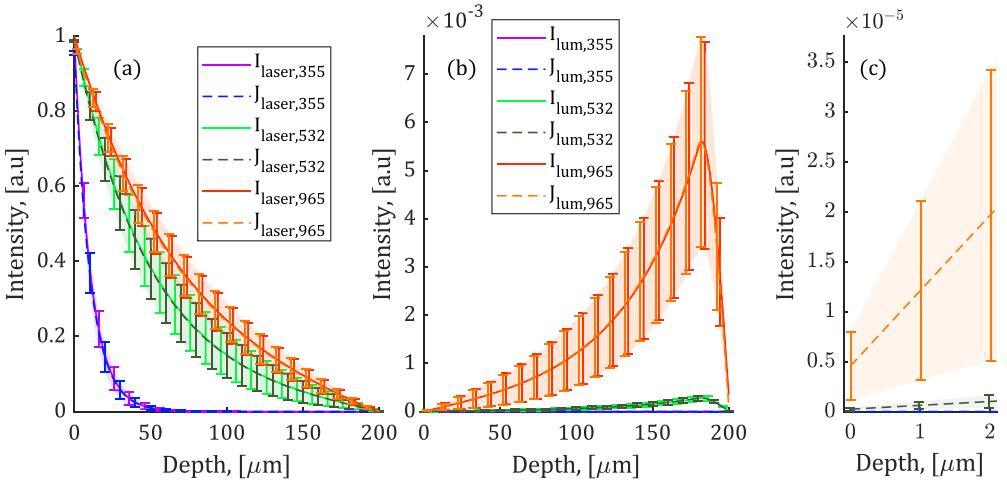

Figure 10. SPS TBC application method. Laser intensity at different depths in the TBC (a) and phosphorescence intensity at different depths with phosphor-doping only in the bottom 20 µm of the 200 µm deep TBC (b). Excitation with UV (355 nm), visible (532 nm) and IR (965 nm) is shown for emission at 550 nm. (c) Shows the phosphor luminescence close to the TBC surface propagating out of the coating.

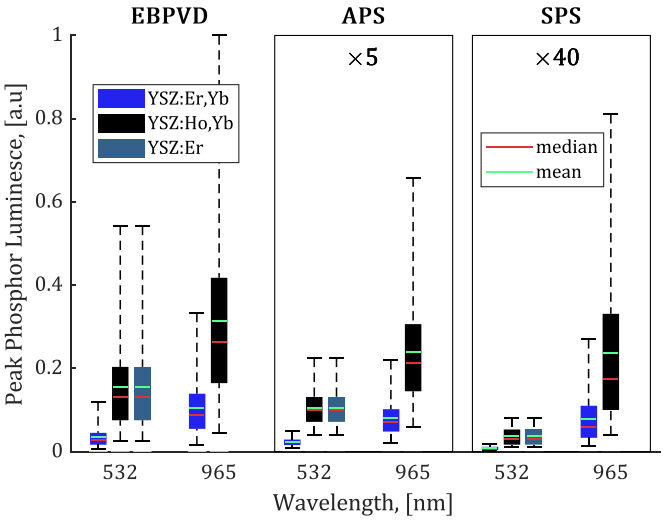

Figure 11. Relative peak phosphor luminescence leaving the TBC with adjustments for the relative peak luminescence of each phosphor using table 2. The plots show the minimum, maximum, lower and upper quartiles, mean, and median values in the peak phosphor luminescence leaving the coating. Note that the luminescence values are multiplied by 5 for the APS coating method and 40 times for the SPS method.

7. Conclusions

The 8YSZ phosphors YSZ:Er,Yb, and YSZ:Ho,Yb were selected for detailed characterisation using upconversion phosphor thermometry. The integrated phosphor luminescence with upconversion excitation was approximately six times brighter for YSZ:Er,Yb and three times brighter for YSZ:Ho,Yb than excitation with 355 nm. The integrated luminescence and peak phosphor luminescence with 532 nm excitation were approximately twice as bright for the YSZ:Er, YSZ:Er,Yb, and YSZ:Ho,Yb phosphors compared with 355 nm excitation.

The phosphors were more temperature sensitive with upconversion thermometry, where YSZ:Er,Yb and YSZ:Ho,Yb were five and two times more temperature sensitive with upconversion excitation, respectively, compared with downconversion. YSZ:Er,Yb and YSZ:Ho,Yb had long rise time components with upconversion excitation, which did not exist with downconversion excitation. This leads to a very low background fluorescence impact on the phosphor decay as the phosphor decay curve is delayed in time from the excitation pulse. This, coupled with the already low background fluorescence generated with upconversion excitation, is promising as it would reduce the interference from impurities in YSZ TBC in situations with an embedded thin phosphor-doped YSZ layer with undoped YSZ on top.

Kubelka–Munk simulations were performed with a 200 μm thick YSZ TBC where the bottom 20 μm was a phosphor layer. Upconversion excitation was shown to result in more phosphor luminosity leaving the TBC than 532 nm and 355 nm excitation for APS, SPS, and EB-PVD, assuming the same excitation efficiency for all wavelengths. Accounting for phosphor excitation efficiency, it was found that upconversion using the YSZ:Ho,Yb phosphor remained the most luminous option.

Upconversion lifetime phosphor thermometry is promising for temperature measurements in a TBC with an embedded phosphor layer owing to the increased temperature sensitivity, reduced fluorescence background influence, and good signal strength compared to downconversion excitation.

Data availability statement

The data cannot be made publicly available upon publication because the cost of preparing, depositing and hosting the data would be prohibitive within the terms of this research project. The data that support the findings of this study are available upon reasonable request from the authors.

Acknowledgments

The authors would like to acknowledge funding from the Swedish Research Council/Swedish Energy Agency through Project 45400-01, the European Commission through Project No. HYFLEXPOWER 884229, and the European Commission through Project No. LAPLAS 852394.

ORCID iD

Henrik Feuk https://orcid.org/0000-0003-2213-458X

References

[1] Cheruvu N S, Chan K S and Viswanathan R 2006 Evaluation, degradation and life assessment of coatings for land based combustion turbines *Energy Mater.* **1** 33–47
[2] Abou Nada F, Lantz A, Larfeldt J, Markocsan N, Aldén M and Richter M 2016 Remote temperature sensing on and beneath atmospheric plasma sprayed thermal barrier coatings using thermographic phosphors *Surf. Coat. Technol.* **302** 359–67
[3] Feist J P and Heyes A L 2009 Photo-stimulated phosphorescence for thermal condition monitoring and nondestructive evaluation in thermal barrier coatings *Heat Transfer Eng.* **30** 1087–95
[4] Steenbakker R J L, Feist J P, Wellman R G and Nicholls J R 2009 Sensor thermal barrier coatings: remote *in situ* condition monitoring of EB-PVD coatings at elevated temperatures *J. Eng. Gas Turbines Power* **131** 1–9
[5] Gentleman M M, Eldridge J I, Zhu D M, Murphy K S and Clarke D R 2006 Non-contact sensing of TBC/BC interface temperature in a thermal gradient *Surf. Coat. Technol.* **201** 3937–41
[6] Gonzalez A Y, Pilgrim C C, Sollazzo P Y, Heyes A L, Feist J P, Nicholls J R, Beyrau F *et al* 2014 Temperature sensing inside thermal barrier coatings using phosphor thermometry *IET & ISA 60th Int. Instrumentation Symp. 2014 (London, 24–26 June 2014)* p 630
[7] Gentleman M M, Lughi V, Nychka A J and Clarke R D 2006 Noncontact methods for measuring thermal barrier coating temperatures *Int. J. Appl. Ceram. Technol.* **3** 105–12
[8] Eldridge J I 2008 Determination of scattering and absorption coefficients for plasma-sprayed yttria-stabilized

zirconia thermal barrier coatings *J. Am. Ceram. Soc.* **91** 1603–11
[9] Zhao S, Li X, Huai X, Cheng K and Zhou X 2018 Experimental study on the scattering and absorption coefficients of thermal barrier coatings at elevated temperatures *Int. J. Heat Mass Transfer* **121** 900–10
[10] Eldridge J I and Wolfe D E 2019 Monitoring thermal barrier coating delamination progression by upconversion luminescence imaging *Surf. Coat. Technol.* **378** 124923
[11] Pilgrim C C, Feist J P and Heyes A L 2013 On the effect of temperature gradients and coating translucence on the accuracy of phosphor thermometry *Meas. Sci. Technol.* **24** 105201
[12] Fouliard Q, Haldar S, Ghosh R and Raghavan S 2019 Modeling luminescence behavior for phosphor thermometry applied to doped thermal barrier coating configurations *Appl. Opt.* **58** D68
[13] Fouliard Q, Ghosh R and Raghavan S 2020 Doped 8% yttria-stabilized zirconia for temperature measurements in thermal barrier coatings using phosphor thermometry *AIAA 2020-0631 Session: Turbines I* (*6–10 January 2020*) (https://doi.org/10.2514/6.2020-0631)
[14] Li Y, Cai T, Yang L, Guo S, Peng D, Zhao X and Liu Y 2020 Effect of oxygen partial pressure on the phosphorescence of different lanthanide ion (Ln^{3+})-doped yttria-stabilised zirconia *Sens. Actuators* B **308** 127666
[15] Shen Y, Chambers M D and Clarke D R 2008 Effects of dopants and excitation wavelength on the temperature sensing of Ln^{3+}-doped 7YSZ *Surf. Coat. Technol.* **203** 456–60
[16] Eldridge J I, Allison S W, Jenkins T P, Gollub S L, Hall C A and Walker D G 2016 Surface temperature measurements from a stator vane doublet in a turbine afterburner flame using a YAG:Tm thermographic phosphor *Meas. Sci. Technol.* **27** 125205
[17] Gao D, Zhang X and Gao W 2012 Tuning upconversion emission by controlling particle shape in NaYF 4: yb^{3+}/Er 3+ nanocrystals *J. Appl. Phys.* **111** 3–8
[18] Wang X, Bu Y, Xiao S, Yang X and Ding J W 2008 Upconversion in Ho^{3+}-doped YbF_3 particle prepared by coprecipitation method *Appl. Phys. B: Lasers Opt.* **93** 801–7
[19] Przybylska D, Ekner-Grzyb A, Grześkowiak B F and Grzyb T 2019 Upconverting SrF_2 nanoparticles doped with Yb^{3+}/Ho^{3+}, Yb^{3+}/Er^{3+} and Yb^{3+}/Tm^{3+} ions—optimisation of synthesis method, structural, spectroscopic and cytotoxicity studies *Sci. Rep.* **9** 1–12
[20] Soares M R N, Ferro M, Costa F M and Monteiro T 2015 Upconversion luminescence and blackbody radiation in tetragonal YSZ co-doped with Tm^{3+} and Yb^{3+} *Nanoscale* **7** 19958–69
[21] Kraft M, Würth C, Palo E, Soukka T and Resch-Genger U 2019 Colour-optimized quantum yields of Yb, Tm Co-doped upconversion nanocrystals *Methods Appl. Fluoresc.* **7** 024001
[22] Guo X, Zhao H, Song H, Zhang R and Combs C 2011 Upconverting phosphor thermometry for high temperature sensing applications *Sens. Transducers* **13** 124–30
[23] Darolia R 2013 Thermal barrier coatings technology: critical review, progress update, remaining challenges and prospects *Int. Mater. Rev.* **58** 315–48
[24] Sun Y, Luo J and Zhu J 2020 Ferroelastic toughening of single crystalline yttria-stabilized t' zirconia: a phase field study *Eng. Fract. Mech.* **233** 107077
[25] Feuk H, Nilsson S and Richter M 2022 Automated phosphor thermometry lifetime calibration of multiple phosphors and emission lines to above 1900 K *Meas. Sci. Technol.* **33** 127003
[26] Brübach J, Dreizler A and Janicka J 2007 Gas compositional and pressure effects on thermographic phosphor thermometry *Meas. Sci. Technol.* **18** 764–70
[27] Brübach J, Feist J P and Dreizler A 2008 Characterization of manganese-activated magnesium fluorogermanate with regards to thermographic phosphor thermometry *Meas. Sci. Technol.* **19** 025602
[28] Voron'ko Y K, Vishnyakova M A, Lomonova E E, Popov A V, Sobol' A A, Ushakov S N and Shukshin V E 2004 Spectroscopy of Yb^{3+} in cubic ZrO_2 crystals *Inorg. Mater.* **40** 502–8
[29] Wang D, Wu W, Tan X, Goodman B A, Xu S and Deng W 2021 Upconversion visible light emission in yb/pr co-doped yttria-stabilized zirconia (Ysz) single crystals *Crystals* **11** 1328
[30] Wei T, Tian Y, Tian C, Jing X, Zhang J, Zhang L and Xu S 2014 Optical spectroscopy and population behavior between 4I_11/2 and 4I_13/2 levels of erbium doped germanate glass *Opt. Mater. Express* **4** 2150
[31] Aarts L, Van Der Ende B M and Meijerink A 2009 Downconversion for solar cells in NaYF4: Er,Yb *J. Appl. Phys.* **106** 023522
[32] Avram D, Tiseanu I, Vasile B S, Florea M and Tiseanu C 2018 Near infrared emission properties of Er doped cubic sesquioxides in the second/third biological windows *Sci. Rep.* **8** 1–12
[33] Brübach J, Janicka J and Dreizler A 2009 An algorithm for the characterisation of multi-exponential decay curves *Opt. Lasers Eng.* **47** 75–79
[34] Fuhrmann N, Brübach J and Dreizler A 2013 Spectral decomposition of phosphorescence decays *Rev. Sci. Instrum.* **84** 4–9
[35] Feuk H, Nilsson S and Richter M 2022 Laser excitation effects in lifetime-based high-speed phosphor thermometry *J. Lumin.* **250** 119106
[36] Feuk H, Sanned D, Richter M and Aldén M 2021 Sources of error for single-shot PMT-based phosphor thermometry in harsh conditions *Meas. Sci. Technol.* **32** 084003
[37] Wang X, Tan X, Xu S, Liu F, Goodman B A and Deng W 2020 Preparation and up-conversion luminescence of Er-doped yttria stabilized zirconia single crystals *J. Lumin.* **219** 116896
[38] Huang F, Liu X, Ma Y, Kang S, Hu L and Chen D 2015 Origin of near to middle infrared luminescence and energy transfer process of Er^{3+}/Yb^{3+} co-doped fluorotellurite glasses under different excitations *Sci. Rep.* **5** 5–10
[39] Pavani K, Suresh Kumar J, Srikanth K, Soares M J, Pereira E, Neves A J and Graça M P F 2017 Highly efficient upconversion of Er^{3+} in Yb^{3+} codoped non-cytotoxic strontium lanthanum aluminate phosphor for low temperature sensors *Sci. Rep.* **7** 1–15
[40] Lüthi S R, Pollnau M, Güdel H U and Hehlen M P 1999 Near-infrared to visible upconversion in Er^{3+} -doped $Cs_3Lu_2Cl_9$, $Cs_3Lu_2Br_9$, and $Cs_3Y_2I_9$ excited at 1.54 μm *Phys. Rev.* B **60** 162–78
[41] Vargas W E and Niklasson G A 1997 Applicability conditions of the Kubelka–Munk theory *Appl. Opt.* **36** 5580
[42] Yang G and Zhao C Y 2015 A comparative experimental study on radiative properties of EB-PVD and air plasma sprayed thermal barrier coatings *J. Heat Transfer* **137** 091024
[43] Blanchard F, Baloukas B, Azzi M, Ettouil F B, Klemberg-Sapieha J E, Moreau C and Martinu L 2022 A comparative study of the optical and microstructural properties of suspension and atmospheric plasma sprayed thermal barrier coatings *Surf. Coat. Technol.* **449** 128949
[44] Debout V *et al* 2007 Investigation of in-flight particle characteristics and microstructural effects on optical properties of YSZ plasma sprayed coatings *High Temp. Mater. Process.* **11** 309–20

[45] Limarga A M and Clarke D R 2009 Characterization of electron beam physical vapor-deposited thermal barrier coatings using diffuse optical reflectance *Int. J. Appl. Ceram. Technol.* **6** 400–9
[46] Fouliard Q, Ghosh R and Raghavan S 2020 Quantifying thermal barrier coating delamination through luminescence modeling *Surf. Coat. Technol.* **399** 126153
[47] Dong J, Bass M, Mao Y, Deng P and Gan F 2003 Dependence of the Yb^{3+} emission cross section and lifetime on temperature and concentration in yttrium aluminum garnet *J. Opt. Soc. Am.* B **20** 1975
[48] Zmojda J, Dorosz D, Kochanowicz M and Dorosz J 2014 Active glasses as the luminescent sources of radiation for sensor applications *Bull. Pol. Acad. Sci.: Tech. Sci.* **62** 393–7
[49] Linganna K, Ju S, Kim B, Han W T, Venkatramu V and Jayasankar C K 2017 Spectroscopic properties of Yb^{3+}-doped silicate glasses *Z. Phys.* **232** 51–60
[50] Tang F, Wang W, Yuan X, Zhu C, Huang J, Ma C, Wang F, Lin Y and Cao Y 2014 Dependence of optical and thermal properties on concentration and temperature for Yb: YAG laser ceramics *J. Alloys Compd.* **593** 123–7